Available online at www.sciencedirect.com
SCIENCE DIRECT®
ELSEVIER
Nuclear Instruments and Methods in Physics Research A 538 (2005) 723–730
NUCLEAR INSTRUMENTS & METHODS IN PHYSICS RESEARCH Section A
www.elsevier.com/locate/nima

# Doppler broadening of positron annihilation radiation: fitting the coincidence spectrum

E. do Nascimento, O. Helene[a,*], C. Takiya[b], V.R. Vanin

[a]*Instituto de Física, Universidade de São Paulo, Caixa Postal 66318, CEP 05315-970, São Paulo, SP, Brazil*
[b]*Departamento de Ciências Exatas, Universidade Estadual do Sudoeste da Bahia, CEP 45083-900, Vitória da Conquista, BA, Brazil*

Received 10 March 2004; received in revised form 9 September 2004; accepted 10 September 2004
Available online 18 October 2004

**Abstract**

The profile of the annihilation radiation in aluminum using positrons from a $^{22}$Na source was observed in a two-HPGe-detectors arrangement. The coincidence photon energy spectrum was fitted using a model function, accounting for both Doppler broadening and detector system response. Intensities of the thermalized positron annihilation with band, 2p, 2s, and 1s electrons, and in-flight positron annihilation were fitted. The binding energies of the 1s, 2s, and 2p electrons and the Fermi cutoff parameters of the band electrons were also fitted.


*PACS:* 02.05.Tt; 07.05.Kf; 29.30.Kv; 71.18.+y; 78.70.Bj

*Keywords:* Doppler broadening; Positron annihilation; Least-squares method; Gamma-ray spectroscopy

## 1. Introduction

Positrons injected into materials are rapidly thermalized before annihilation with surrounding electrons, when, in most cases, two gamma-rays are emitted. These gamma-rays are Doppler shifted due to the center of mass velocity of the electron–positron pair. Since the center of mass velocity depends on the electron momentum, the measurement of the gamma-ray energies can provide information about the electron momentum distribution. This technique has been successfully used in the study of materials, especially after the introduction of a second detector to the experimental setup by Lynn et al. [1].

The energies of the emitted photons are given by

$$E_{\pm} \cong m_0c^2 - \frac{B_i}{2} \pm \frac{p_z c}{2} \quad (1)$$

where $m_0c^2$ is the electron rest energy, $B_i$ is the binding energy of the annihilated electron, and $p_z$

*Corresponding author. Tel.: +55 11 3091 6858; fax: +55 11 3091 6832.
*E-mail address:* otaviano@if.usp.br (O. Helene).

0168-9002/$ - see front matter © 2004 Elsevier B.V. All rights reserved.
doi:10.1016/j.nima.2004.09.013

is the longitudinal component of the electron momentum.

When just one detector is used, the annihilation radiation yields a gamma-ray peak at 511 keV broadened both by the Doppler effect given by

$$\frac{\sqrt{\langle p_z^2\rangle}c}{2} \quad (2)$$

where $\langle\rangle$ stands for mean value, and by the detector response function. When two detectors are used, a coincidence energy spectrum with a peak at 511 keV × 511 keV is obtained. Calling $E_1$ and $E_2$ the main axes of the coincidence energy spectrum, the detector system response function broadens the peak along the $E_1 = E_2$ direction, while along the $E_1 + E_2 \cong 2mc^2$ direction both the Doppler effect and the detector response contribute to the broadening. Since electrons of different shells can be annihilated, the coincidence peak is a superposition of different peaks slightly displaced along the $E_1 = E_2$ direction by the electron binding energies.

Usually, in the analysis of coincidence experiments, the two-dimensional coincidence spectrum is reduced to a projected one-dimensional spectrum by calculating the marginal distribution along the $E_1 + E_2 =$ constant direction, that is, the projection of the data in the coincidence spectrum in a perpendicular plane along one of its diagonals. In that procedure, the horizontal axis is usually given in units of the electron momentum (see, for instance, Refs. [2–4]). Comparing this projection with the results provided by just one detector, some improvements are obtained: the peak to background ratio is increased by a few orders of magnitude and the Doppler broadening to combined detectors resolution ratio is increased by $\sqrt{2}$.

In spite of these improvements, some information is lost after the projection. When projected, some events due to the detectors secondary effects that were out of the region of interest in the coincidence spectrum are interwoven with the main signal. Also, events due to positron annihilation with conduction and bound electrons, which were slightly separated by the binding energy in the two-dimensional coincidence spectrum, are summed together. Thus, the analysis of the two-dimensional energy spectrum can reveal details that are hidden in the one-dimensional projection. In this paper we choose to analyze the coincidence spectrum.

The Doppler-broadened gamma-ray spectra are usually analyzed as follows. In a first step, the electron momentum distribution and the expected gamma-ray spectrum are theoretically calculated. Next, one calculates the convolution of the obtained spectrum with the system response function, which is compared with the projected spectrum. In this paper we opted for another procedure. In a first step, the convolution of the detector response function with empirical functions to represent the gamma-rays emitted after annihilation was calculated; all these functions were parameterized. Next, the parameters were fitted to the coincidence spectrum using the least-squares method. The advantage of this approach is that the fitted parameters can be compared with other experimental results and theoretical values. The handicap of the method is the difficulty in choosing suitable functions to model the gamma-ray energy distribution.

The main aim of this paper is to give a contribution to the statistical analysis of the experimental data of the Doppler broadening of positron annihilation radiation.

## 2. Experiment and the model function

### 2.1. Experimental

The annihilation gamma-rays were measured by two HPGe detectors in diametrically opposed positions and separated by 15 cm, with a $4 \times 10^5$ Bq $^{22}$Na source placed between two 2 mm thick aluminum sheets (99.999% pure and annealed for 6 h at 600 °C). The coincidence time window was set to 180 ns. An $^{192}$Ir source was simultaneously measured to provide the detector energy calibrations and to follow any energy drift during the experiment. The measurement run lasted for 200 h, when $1.5 \times 10^7$ events in the peak region were accumulated. The contour plot of the coincidence spectrum is presented in Fig. 1, where the crest along the line $E_1 + E_2 \cong 1022$ keV is mainly due

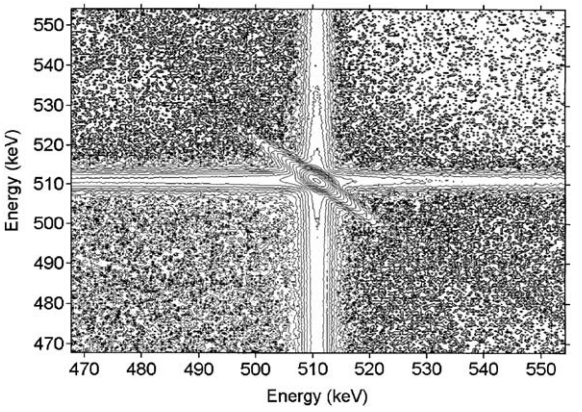


Fig. 1. Contour plot of the coincidence energy spectrum of the observed gamma-rays.

to at-rest positron annihilation with core and band electrons. The ridges parallel to the principal axes come from the coincidence between an annihilation gamma-ray with a Compton scattered gamma-ray, coming from either the other annihilation radiation or the 1274 keV gamma-ray following $^{22}$Na decay. The complete explanation of the spectrum, however, requires many more details, given below.

### 2.2. Model function

The measured spectrum was modeled by a function which was fitted, after convolution with the detector system response function (see Section 2.3), to the experimental histogram. The model included at-rest positron annihilation with core and band electrons, and in-flight positron annihilation. The model function was determined from a qualitative analysis of the experimental data and published theoretical results [2–4].

Positron annihilation with band electrons was fitted by three arcs of parabola and one Gaussian along the line $E_1 + E_2 = 1022$ keV, given by

$$f_b = \sum_{i=1}^{3} C_i(E_1 - E_2 - \alpha_i)(E_1 - E_2 + \alpha_i) + \frac{A_v e^{(-(E_1-E_2)^2)/2\sigma_v^2}}{\sqrt{2\pi}\sigma_v} \quad (3)$$

where $\alpha_i$ are the Fermi cutoff parameters ($C_i = 0$ when $|E_1 - E_2| > \alpha_i$). The three arcs of parabola take into account the more prominent effects of positron annihilation with band electrons seen in the experimental spectrum and expected from theoretical calculations, and enable the fit of the three Fermi cutoff parameters; the Gaussian term takes into account a small contribution that extends beyond the Fermi cutoff parameters. The parameters $C_i, \alpha_i, A_v$, and $\sigma_v$ were fitted.

Theoretical calculation of positron annihilation with 1s electrons shows just one maximum in the analyzed region, being about four orders of magnitude smaller than annihilation with band electrons [3,4]. In consequence, annihilation with 1s electrons was represented by just one Gaussian peak given by

$$f_{1s} = \frac{A_{1s} e^{(-(E_1-E_2)^2)/2\sigma_{1s}^2}}{\sqrt{2\pi}\sigma_{1s}} \quad (4)$$

along the line $E_1 + E_2 + B_{1s} = 2m_0c^2$, where $B_{1s}$ is the 1s electron binding energy. The fitted parameters are $A_{1s}$, $\sigma_{1s}$, and $B_{1s}$.

Positron annihilation with 2s electrons has a dominant maximum in the region $p < 20 \times 10^{-3} m_0 c$ and a large tail that extends beyond $p \sim 60 \times 10^{-3} m_0 c$ [2–4]. In consequence, we represent this annihilation by two Gaussians

$$f_{2s} = \frac{A_{2s} e^{(-(E_1-E_2)^2)/2\sigma_{2s}^2}}{\sqrt{2\pi}\sigma_{2s}} + \frac{A'_{2s} e^{(-(E_1-E_2)^2)/2\sigma_{2s}^2}}{\sqrt{2\pi}\sigma'_{2s}} \quad (5)$$

along the line $E_1 + E_2 + B_{2s} = 2m_0c^2$, where $B_{2s}$ is the binding energy of the 2s electrons. $B_{2s}$, $A_{2s}$, $A'_{2s}$, $\sigma_{2s}$, and $\sigma'_{2s}$ were fitted.

Positron annihilation with 2p electrons has just a maximum in the analyzed region [2,3]. Thus, it was fitted by just one Gaussian

$$f_{2p} = \frac{A_{2p} e^{(-(E_1-E_2)^2)/2\sigma_{2p}^2}}{\sqrt{2\pi}\sigma_{2p}} \quad (6)$$

along the line $E_1 + E_2 + B_{2p} = 2m_0c^2$. In this case we fitted $A_{2p}$, $\sigma_{2p}$, and the binding energy $B_{2p}$. Since positron annihilation radiation with $2p_{1/2}$ and $2p_{3/2}$ electrons show the same dependence on the electron momentum, they cannot be separated in the fit.

In-flight positron annihilation has been observed in recent experiments [5–9] and was considered in the fitting. When a positron annihilates in-flight with a low-momentum electron, two gamma-rays are emitted with energies $E_1$ and $E_2$ given by

$$E_{1,2} \cong m_0c^2 + \frac{p^2/2m_0 - B}{2} \pm \frac{p_\parallel c}{2} \tag{7}$$

where $p$ is the total positron momentum, $p_\parallel$ is its component parallel to the gamma-ray emission direction, and $B$ is the electron binding energy. When $p_\parallel$ takes its extreme value $p$, then $E_1$ and $E_2$ take their extreme values, too. Neglecting $B$ in Eq. (7), the extreme values of $E_1$ and $E_2$ are given by

$$E^{\mathrm{m}}_{1,2} = m_0c^2 + \frac{p^2}{4m_0} \pm \frac{pc}{2}. \tag{8}$$

This pair of equations can be written as

$$\left(E^{\mathrm{m}}_1 - \frac{3}{2}m_0c^2\right)^2 + \left(E^{\mathrm{m}}_2 - \frac{3}{2}m_0c^2\right)^2 = \frac{p^4}{8m_0^2} + \frac{m_0^2c^4}{2}. \tag{9}$$

Consequently, for small positron momentum ($p \ll mc$), corresponding to points near the 511 keV × 511 keV peak, this equation describes a circular arc which is barely seen in Fig. 1. Fig. 2 shows a projection of the spectrum along the radial distance, measured from the center of the circle $E_1 = E_2 = 3m_0c^2/2$, summing the counts in the regions identified in the figure inset. This one-dimensional projected spectrum shows a clear bump just above 1022 keV, confirming the existence of a circular ridge in the coincidence spectrum.

Thus, the last component included in the fit is the in-flight positron annihilation, empirically approximated by

$$f_{\mathrm{f}} = \frac{A_{\mathrm{f}} e^{-\lambda d} e^{(-(E_1-E_2)^2)/2\sigma_{\mathrm{f}}^2}}{\sqrt{2\pi}\sigma_{\mathrm{f}}} \tag{10}$$

for points $(E_1, E_2)$ inside the circle given by Eq. (9), where $d$ is the distance (in energy) between $(E_1, E_2)$ and the circular arc given by

$$d = \frac{m_0c^2}{\sqrt{2}} - \sqrt{\left(E_1 - \frac{3m_0c^2}{2}\right)^2 + \left(E_2 - \frac{3m_0c^2}{2}\right)^2}. \tag{11}$$

For points outside the circle the contribution of in-flight positron annihilation is zero. The empirical parameters $A_{\mathrm{f}}, \lambda$, and $\sigma_{\mathrm{f}}$ were fitted.

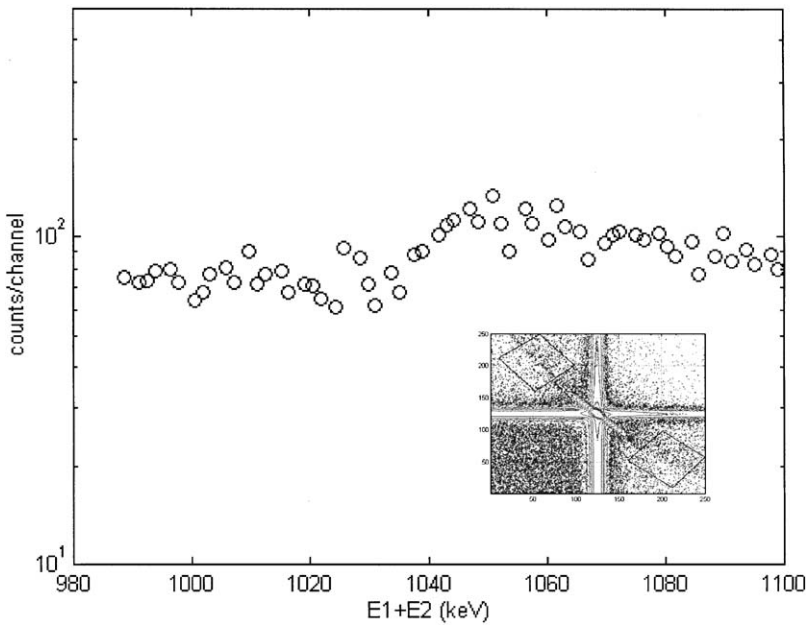


Fig. 2. Radial projection of the selected regions (shown in the inset) of the coincidence spectrum; see text for definition of the radial coordinate.

### 2.3. Response function and background

The detectors response functions are given by a Gaussian part and a non-Gaussian part. The Gaussian part has two parameters corresponding to the detectors' resolution. The non-Gaussian part of the detector response functions, due to ballistic defects and incomplete charge collection, was fitted by two internal ($E<E_\gamma$) and two external ($E>E_\gamma$) exponential queues for each detector, with a total of 16 parameters.

Two internal and two external ridges along the lines $E_1 = 511\,\text{keV}$ and $E_2 = 511\,\text{keV}$, with amplitudes proportional to the peak intensity, were included in the fit to take into account photons from the scattering of annihilation or 1274 keV gamma-rays in coincidence with an annihilation gamma-ray, corresponding to four intensity parameters. It was assumed that the number of background counts in channel $(i_0, j_0)$ is proportional to the product of the total number of counts in the ridges along the line $i = i_0, j > j_0$ by the total number of counts along the line $j = j_0, i > i_0$; the single fitted parameter was the proportionality factor.

Since the two detectors were not identical, the relative efficiency was approximated by $1 + a_1(E_1 - 511\,\text{keV}) + a_2(E_2 - 511\,\text{keV})$, where $a_1$ and $a_2$ were fitted. Three parameters corresponding to the peak position in the two energy axes, and the angular inclination of the $E_1 + E_2 = 2m_0c^2$ line relative to the main axes were fitted.

Finally, the simultaneous detection by each detector of one annihilation photon scattered in the other detector, which results in events located along the $E_1 + E_2 \approx 1022\,\text{keV}$ line, was taken into account. This secondary detection phenomenon was assumed constant in the analyzed region and fitted by just one parameter, its intensity.

## 3. Results

The fitting function is the convolution of the model function plus the background with the detector system response function. The function was fitted to an 87 keV × 87 keV region around the two-photon annihilation peak using the Gauss–Marquardt method of nonlinear parameter estimation [10,11]. The required partial derivatives were evaluated numerically. Uncertainties and covariances of the parameters were calculated using the procedure described in Refs. [10,12].

The $\chi^2$ value was calculated using the equation

$$\chi^2 = \sum_{i,j} \frac{(n_{ij} - F_{ij})^2}{F_{ij}} \tag{12}$$

where $n_{ij}$ is the number of observed events in channel $(i,j)$ of the two-dimensional spectrum, and $F_{ij}$ is the fitted function.

The obtained $\chi^2$ value was $6.9615 \times 10^4$ for $6.2448 \times 10^4$ degrees of freedom (52 parameters fitted to 250 × 250 channels), giving a reduced $\chi^2$ of 1.11.

The most interesting results are given in Table 1. The relative intensities of positron annihilation with band and core electrons agree with other works [2–4]. The fitted binding energies of 2p, 2s, and 1s electrons, 70(9) eV, 0.12(5) keV, and 1.45(13) keV, agree well with their recommended values, respectively 73 eV, 0.118 keV, and 1.56 keV [13]. The adjusted Fermi cutoff parameters agree with the values given in Ref. [4].

Fig. 3 shows the fitted coincidence spectrum. Fig. 4 shows the fitted and experimental projected Doppler profiles, including the 1s, 2s, 2p, band electron annihilations, and in-flight positron annihilation components.

Table 1
Selection of fitted parameters: relative intensity of positron annihilation with band, 2p, 2s, and 1s electrons; in-flight annihilation intensity; the three Fermi cutoff parameters; and 2p, 2s, and 1s electron binding energies

| | |
|---|---|
| Band annihilation (%) | 91.9(13) |
| 2p annihilation (%) | 5.42(32) |
| 2s annihilation (%) | 2.6(12) |
| 1s annihilation (%) | 0.0145(25) |
| In-flight annihilation[a] (%) | 0.066(3) |
| $\alpha_1(10^{-3}m_0c)$ | 6.820(8) |
| $\alpha_2(10^{-3}m_0c)$ | 10.87(9) |
| $\alpha_3(10^{-3}m_0c)$ | 16.24(11) |
| 2p binding energy (keV) | 0.070(9) |
| 2s binding energy (keV) | 0.12(5) |
| 1s binding energy (keV) | 1.45(13) |

[a]In the fitted region.

The squares of the relative residues given by

$$\Delta_{ij} = \frac{(n_{ij} - F_{ij})^2}{F_{ij}} \quad (13)$$

are shown in Fig. 5, where no special feature stands out against the statistical fluctuation.

## 4. Discussion and conclusion

The annihilation components fitted to the observed peak span several orders of magnitude and require 52 different parameters in the least-squares procedure, which were described in Sections 2.2 and 2.3. The experimental data allowed a reliable determination of almost all the fitted parameters; the most difficult cases and the exceptions will be noted below.

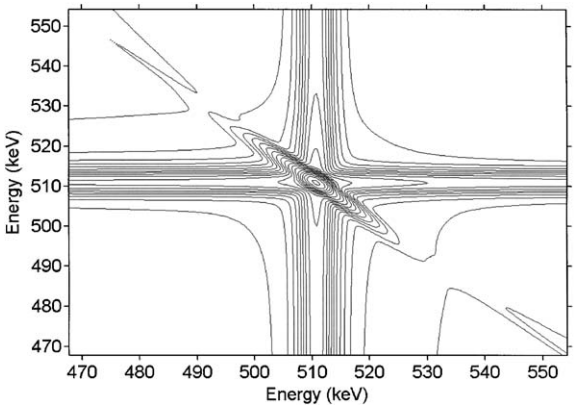


Fig. 3. Fitted coincidence histogram, corresponding to Fig. 1.

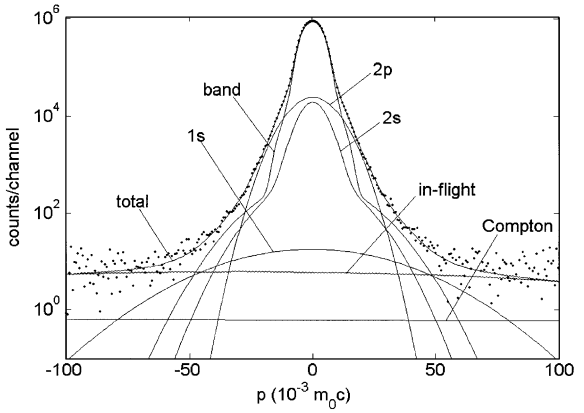


Fig. 4. Fitted and experimental Doppler profiles, including the 1s, 2s, 2p, band electron annihilations, and in-flight positron annihilation contribution.

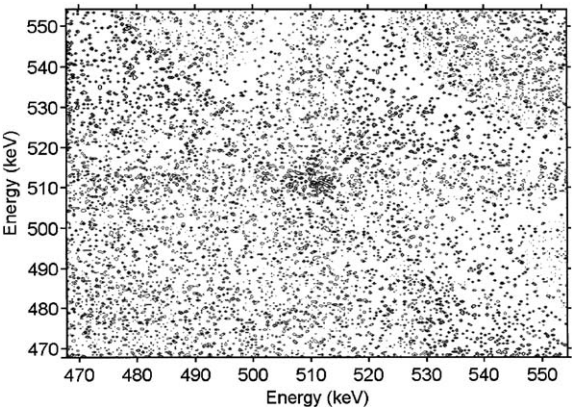


Fig. 5. Contour plot of the relative residue spectrum.

Surprising as it may seem, the 1s bound electron annihilation intensity, although blurred with the strong band electron annihilation intensity, can be extracted precisely. This happens because an important fraction of gamma-rays from these events falls in an energy region where there are not many events from band electron annihilation. First, the 1s annihilation gamma-ray energies are displaced from the dominant events, annihilation with band electrons distributed around the line $E_1 + E_2 \approx 1022\,\text{keV}$, by the binding energy, therefore lying around the line $E_1 + E_2 = 2m_0c^2 - B_{1s}$. Additionally, the Doppler shift for annihilation with 1s electrons tends to be larger than with band electrons due to the higher momentum of the electron, resulting in many annihilation gamma-rays with energies very different from 511 keV. Fig. 6 shows the squares of the weighted residues in a fit where annihilation with the 1s bound electron was not included in the model, showing meaningful residues in two regions, with energy sum smaller that 1022 keV and displaced from the 511 keV × 511 keV main peak, exactly in the region characteristic of annihilation with 1s electrons; hence, the good detector resolution

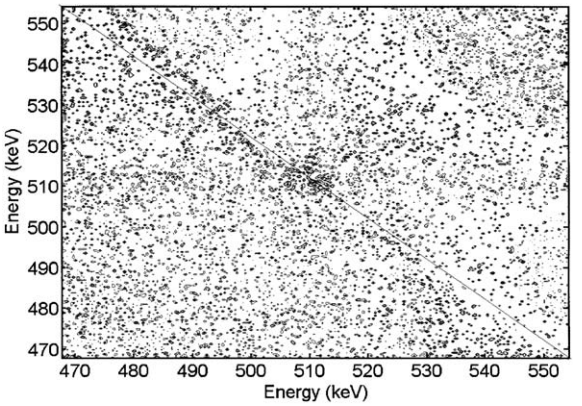


Fig. 6. Contour plot of the relative residue spectrum when 1s annihilation is excluded from the model function (see text for details).

and counting statistics of the experiment allowed fair observation of the phenomenon. From the statistical point of view, this is reflected in a large difference in $\chi^2$ when including or not 1s annihilation in the model function; in this experiment, $\chi^2$ decreased by 480 when reducing the number of degrees of freedom by three, corresponding to the inclusion of the parameters $A_{1s}$, $\sigma_{1s}$, and $B_{1s}$ (see Eq. (4)) in the fit.

Two other weak components, representing phenomena secondary to this work, could also be fitted because they show up themselves in energy regions away from the dominant peak. One of them describe the simultaneous detection by each detector of one annihilation photon scattered in the other, which are located along $E_1 + E_2 = 1022\,\text{keV}$, and can be clearly observed only far from the main peak. The other is the in-flight positron annihilation, also very weak, which was resolved from the other structures due to its typical circular profile in the gamma–gamma coincidence energy plan, extending beyond the region dominated by the 511 keV × 511 keV peak.

The parameters that cannot be extracted reliably are the intensities and widths of the two Gaussian functions fitted to take into account annihilation with 2s electrons, described by Eq. (5). However, there is no reason to observe annihilation with 2p and 1s electrons and not with 2s electrons; since the fitted parameters agree well with expectations, it was kept in the fitting procedure. On account of the node in the radial wave function of 2s electrons, the momentum wave function must have two components, which led to the choice of two Gaussians to model the annihilation intensity.

In conclusion, we have found that a complete statistical analysis of the coincidence Doppler annihilation radiation spectrum is possible and provides some parameters and their uncertainties that are difficult to obtain from a projected spectrum. The electron binding energies and Fermi cutoff parameters were determined and the obtained results agree well with published values, corroborating the procedure. Better model functions will improve this procedure.

## Acknowledgements

The authors would like to thank Drs. M.T.F. da Cruz, M. Moralles, P.R. Pascholati and J.Y. Zevallos-Chavez. This work was sponsored by FAPESP and CNPq Brazilian agencies and IAEA under contract BRA10368.

## References

[1] K.G. Lynn, J.R. MacDonald, R.A. Boie, L.C. Feldman, J.D. Gabbe, M.F. Robbins, E. Bonderup, J. Golovchenko, Phys. Rev. Lett. 38 (1977) 241.
[2] V.J. Ghosh, M. Alatalo, P. Asoka-Kumar, B. Nielsen, K.G. Lynn, A.C. Kruseman, P.E. Mijnarends, Phys. Rev. B 61 (2000) 10092.
[3] P.E. Mijnarends, A.C. Kruseman, A. van Veen, H. Schut, A. Bansil, J. Phys.: Condens. Matter 10 (46) (1998) 10383.
[4] Z. Tang, M. Hasegawa, Y. Nagai, M. Saito, Y. Kawazoe, Phys. Rev. B 65 (2002) (Art. No. 045108).
[5] A.W. Hunt, D.B. Cassidy, F.A. Selim, R. Haakenaasen, T.E. Cowan, R.H. Howell, K.G. Lynn, J.A. Golovchenko, Nucl. Instr. and Meth. B 164 (2000) 44.
[6] M.H. Weber, A.W. Hunt, J.A. Golovchenko, K.G. Lynn, Phys. Rev. Lett. 83 (1999) 4658.
[7] A.W. Hunt, D.B. Cassidy, F.A. Selim, R. Haakenaasen, T.E. Cowan, R.H. Howell, K.G. Lynn, J.A. Golovchenko, Nature 402 (1999) 157.
[8] A.W. Hunt, D.B. Cassidy, P.A. Sterne, T.E. Cowan, R.H. Howell, K.G. Lynn, J.A. Golovchenko, Phys. Rev. Lett. 86 (2001) 5612.

[9] A.W. Hunt, M.H. Weber, J.A. Golovchenko, K.G. Lynn, App. Surf. Sci. 149 (1999) 282.
[10] IAEA TECDOC, Update of X-ray and Gamma-ray Decay Data Standards for Detector Calibration and Other Applications, to be published.
[11] D.W. Marquardt, J. Soc. Appl. Math. 11 (1963) 431.
[12] V.R. Vanin, G. Kenchian, M. Moralles, O. Helene, P.R. Pascholati, Nucl. Instr. and Meth. A 391 (1997) 338.
[13] R.B. Firestone, V.S. Shirley, Table of Isotopes, vol. II. Wiley, Berlin, 1996.